

Single-shot pump-probe technique by the combination of an echelon and a grating with a time window of 109 ps

Tianchen Yu ^a, Junyi Yang ^{a, *}, Zhongguo Li ^b, Xingzhi Wu ^c, Yu Fang ^c, Yong Yang ^{d, *}, Yinglin Song ^{a, *}

^aSchool of Physical Science and Technology, Soochow University, Suzhou 215006, China

^bSchool of Electronic and Information Engineering, Changshu Institute of Technology, Changshu 215500, China

^cJiangsu Key Laboratory of Micro and Nano Heat Fluid Flow Technology and Energy Application, School of Physical Science and Technology, Suzhou University of Science and Technology, Suzhou 215009, China

^dSchool of Optoelectronic Science and Engineering, Soochow University, Suzhou 215006, China

***Corresponding author**

E-mail address: yjy2010@suda.edu.cn (Junyi Yang), yangy@suda.edu.cn (Yong Yang)
ylsong@suda.edu.cn (Yinglin Song)

Abstract

In this study, we report a single-shot pump-probe technique with a large time window of ~ 109 ps and accurate imaging, by using a combination encoding strategy of an echelon and a grating. The obtained time window exceeds the maximum reported values by using an angle beam or echelon encoding strategy. The validity of this technique is demonstrated by studying the two-photon absorption process of ZnSe and the excited-state absorption process of a symmetrical phenoxazinium bromine salt. The measured average minimum time resolution is ~ 855 fs, and the minimum relative transmittance change that can be detected in a single-shot is $\sim 0.75\%$. The factors influencing the time resolution and the possibility of further improving the experimental setup are also discussed.

Keywords: Pump-probe technique, Single-shot, Grating, Echelon

1. Introduction

The pump-probe technique is a powerful tool for diagnosing ultrafast dynamics in all kinds of materials. However, this technique is not suitable for the diagnosis of many irreversible ultrafast phenomena, such as photodissociation [1, 2], phase transition [3], laser ablation [4] and explosion [5], which are limited by the repeated excitation of multiple pulses. In addition, for a long-period measurement, fluctuations in energy from pulse to pulse can increase the noise in the entire pump-probe trace. Therefore, to obtain an adequate signal-to-noise ratio, thousands of pulses must be averaged.

A variety of single-shot pump-probe techniques have been proposed. In general, a single-shot pump-probe technique encodes the time delay into a single pulse using spatial or spectral strategies. Currently, the commonly used encoding strategies include the angle beam encoding strategy [1, 2, 6-8], spectral encoding strategy [9-12], and echelon encoding strategy [3, 5, 13-16]. The angle beam encoding strategy utilizes the crossed line focus of the pump beam and probe beam on the sample plane, and the time delay is encoded along the focal line. Using this strategy, the maximum time window reaches 60ps [8]. However, a high homogeneity and a large sample area are required for the angled beam encoding strategy. The spectral encoding strategy uses a linear chirped pulse, and the sample dynamic information is recorded by the different spectral components of the chirped pulse. A spectral encoding strategy can obtain a high acquisition rate because no camera is required for imaging, and the time window

depends on the width of the chirped pulse. Therefore, the longest time window can reach more than 100 ps [12]. However, the minimum time resolution $\tau_R = \sqrt{\tau_0 \tau}$ depends on the transform-limited pulse τ_0 and the chirped pulse τ , so there is a trade-off between a large time window and a short time resolution [10]. In addition, an oscillation pattern near the origin of the spectral encoded dynamic trace may distort the actual dynamic trace [12]. For the echelon encoding strategy, the probe pulse is encoded as a subpulse chain by the reflection or transmission echelon. The step difference and the echelon height (total step difference) determine the minimum time resolution and the time window, respectively. This approach results in a well-calibrated time delay for the echelon encoding strategy. However, this strategy faces the image blurring problem when a large time window is needed. This is due to the large time window requiring a high echelon height. For example, a 100 ps time window requires the echelon height to be at least 1.5 cm for a reflection echelon. This makes it difficult to accurately image all the step surfaces simultaneously on an image plane. Therefore, the maximum time window reported by the echelon encoding strategy is ~ 37.7 ps [15], which is shorter than that of the other two strategies.

In addition to the above encoding strategies, the use of a grating or a digital micromirror device (DMD) has shown promise [17-19]. However, few studies on this topic exist, and the time window, to the best of our knowledge, has not exceed 30 ps. In this work, therefore, we propose a single-shot pump-probe technique with a large time window using a combination encoding strategy. A combination of a reflection echelon and a commercial grating is used to spatially encode the single probe pulse, and a time window of ~ 109 ps is obtained with accurate imaging. This time window exceeds the current reported values of the angle beam encoding strategy or the echelon encoding strategy. To demonstrate this technique, we studied the ultrafast two-photon absorption process of ZnSe and the long-life excited-state absorption process of a symmetrical phenoxazinium bromine salt.

2. Experimental setup

A schematic of the single-shot pump-probe technique is shown in Fig. 1. A mode-locked Yb: KGW-based fiber laser (1030 nm, 190 fs FWHM, 20 Hz) was used as the laser source. The laser output is frequency doubled to 515 nm for this experiment. The laser beam is divided into a strong pump beam and a weak probe beam using a beam splitter (BS₁). The optical path of the pump beam is adjusted by a time delay stage, and the

pump beam is focused on the sample by lens L_9 ($f = 500$ mm). The energy of the pump and probe beam is adjusted by the neutral density attenuator (ND). The probe beam is expanded to a beam spot approximately 50 mm in diameter. Apertures A_1 and A_2 intercepted the central part of the beams. A reflection echelon (RE) spatially encodes the probe pulse as two subpulses in the step direction (y -direction). As shown in the upper dotted box, the RE consists of two steps with a step difference Δd of 8 mm. Therefore, at a normal incidence, the RE can encode a time delay of $2\Delta d/c = 53.33$ ps between the two subpulses in the y -direction, where c is the light speed. The encoded probe beam then illuminates a ruled grating (G) by a beam splitter (BS_2). The groove direction of the grating is perpendicular to the step direction of the echelon. As shown in the lower dotted box, the grating size is 12.5×25 mm² with a ruled area of 11.5×24 mm² and 75 grooves per mm. At an incident angle that is approximately twice the blaze angle θ_b (22.02°), the direction of the geometric reflection beam is parallel to the grating normal, and a set of time delays is introduced along the grating length (x -direction).

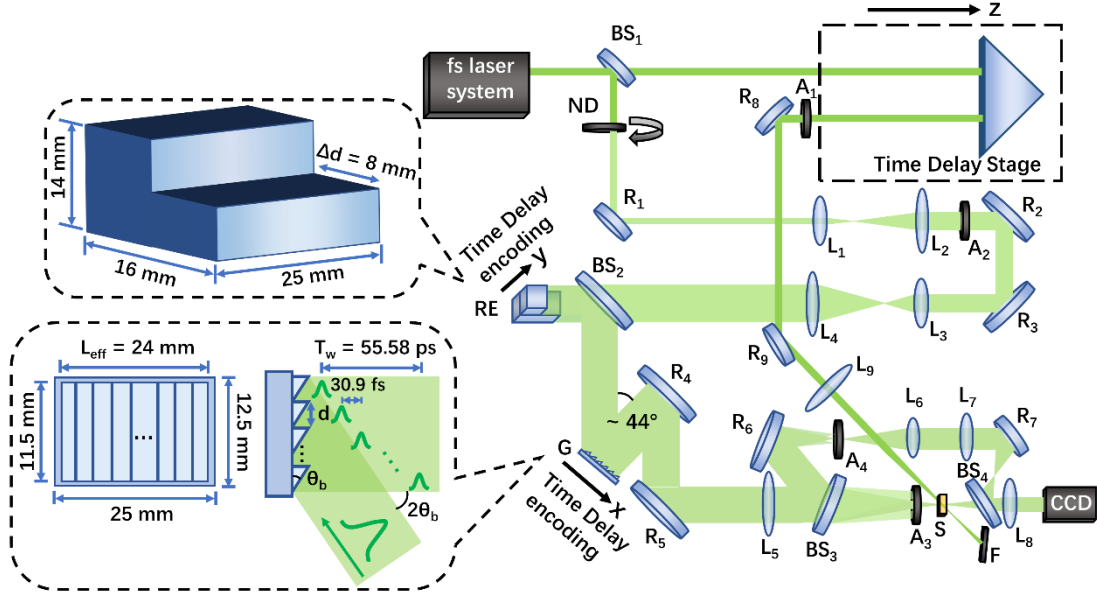


Fig. 1. Schematic of the single-shot pump-probe technique. BS_1 - BS_4 : beam splitter; R_1 - R_9 : mirror; L_1 - L_9 : lens; RE: reflection echelon; G: grating. A_1 - A_4 : apertures; ND: neutral density attenuator; S: sample plane (focal plane); F: flapper; CCD: charge coupled device; top dotted box: schematic of the RE; Δd : step difference; lower dotted box: grating size and spatial encoding; θ_b : blaze angle; L_{eff} : effective length of the grating; d : groove width; T_w : time window.

Therefore, the ruled grating further spatially encodes the two parallel subpulses in

the x -direction. The encoded time window T_w of each subpulse can be calculated by:

$$T_w = L_{eff} \sin(2\theta_b)/c \quad (2-1)$$

Here, L_{eff} is the effective length of the grating. This approach is somewhat similar to the angle beam encoding strategy. However, the time delay is encoded on the grating plane in our geometry instead of on the sample surface. From Eq. (2-1), to obtain a large time window, we need to increase the effective length L_{eff} and choose a large blaze angle θ_b . As shown in Fig. 2(a), the calculated time window of the grating increases with L_{eff} and θ_b . In our experiment, a time window T_w of ~ 55.58 ps can be obtained (indicated by the asterisk) with $L_{eff} = 24$ mm and $\theta_b = 22.02^\circ$. However, for the ruled grating, we need to consider the ratio r_s of the illumination area to the groove area. In our configuration, the ratio can be calculated by $r_s = 1 - 2(\sin \theta_b)^2$. As shown in Fig. 2(b), a larger θ_b will result in a lower illumination ratio r_s . In our experiment, r_s is $\sim 72\%$ (indicated by the asterisk). Therefore, a ruled grating with an effective length L_{eff} of 24 mm and a blaze angle θ_b of 22.02° is suitable for obtaining both a large time window T_w and a high illumination ratio r_s . The encoded time interval Δt can also be calculated by $\Delta t = d \sin(2\theta_b)/c$ with groove width d . In our experiment, the time interval Δt is ~ 30.9 fs which is shorter than the pulse width of 190 fs. Therefore, this time interval is not the minimum time resolution in our experiment.

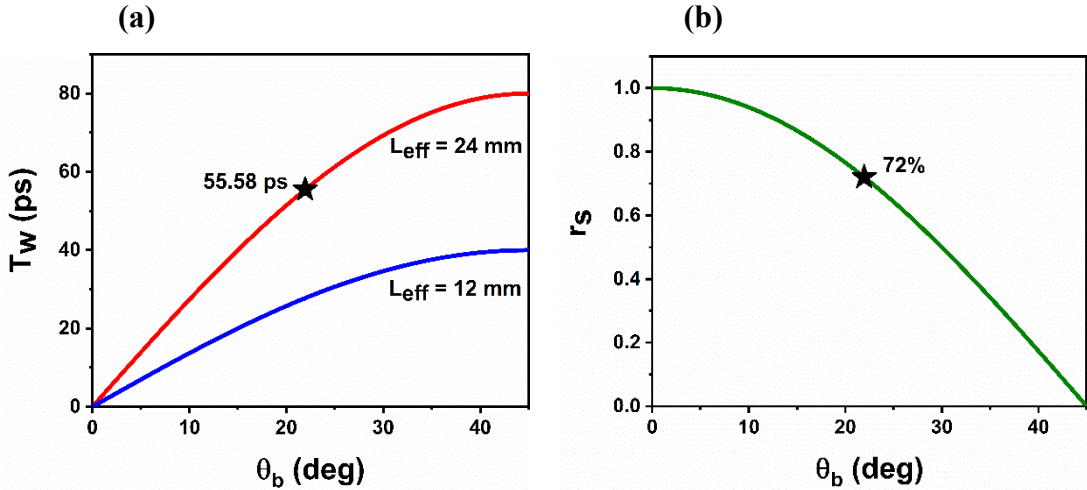


Fig. 2. (a) Calculated time window T_w of the grating with the effective length L_{eff} and the blaze angle θ_b ; (b) illumination ratio r_s of the groove with the blaze angle θ_b .

Overall, with the combination of the reflection echelon RE and the ruled grating G,

a two-dimensional spatial encoding with a total time window of ~ 109 ps is generated. In addition, there is a time overlap of ~ 2.25 ps in the y -direction, considering that the time window for each subpulse is ~ 55.58 ps and the time delay is ~ 53.33 ps. The encoded probe beam is focused by lens L_5 ($f = 250$ mm) to interrogate the pumped area and is imaged on a CCD (spinnaker, 16 bit, 2448×2048 pixels, $3.45 \times 3.45 \mu\text{m}^2$ each pixel) using lens L_8 ($f = 80$ mm). The exposure time of the CCD is set to $50000 \mu\text{s}$ for single-shot acquisition. In addition, a reference beam is divided using a beam splitter (BS_3) and imaged on the CCD reduced by a factor of 2 by lenses L_6 ($f = 50$ mm) and L_7 ($f = 100$ mm), and the reference image is inverted. The reference image is used to monitor the spatial fluctuation of the pulse energy. In our configuration, the grating surface is accurately imaged on the CCD. Therefore, dynamic information can be extracted while avoiding the image blur problem in the traditional echelon encoding strategy since spatial encoding is completed at the grating plane. Moreover, to account for the diffraction of grating G , filtering aperture A_3 is placed in front of sample plane S (focal plane) at a distance of 6 cm. Similarly, a filtering aperture A_4 is placed on the focal plane of the reference path. The diffraction light of the grating follows the following equation:

$$m\lambda = d(\sin \alpha + \sin \beta) \quad (2-2)$$

where λ is the wavelength, m is the diffraction order, and α and β represent the incidence and diffraction angle, respectively. In the condition $\beta = 0$, the separation between the diffraction orders is $\Delta L = \lambda f / d$, where f is the focal length of lens L_5 . In our experiment, ΔL is ~ 0.97 cm and the probe spot size is ~ 5.76 mm in the x -direction at a distance of 6 cm from the focal plane. Therefore, the filtering aperture A_3 with an aperture diameter of 1.10 cm is used to filter the diffractions.

3. Experimental results

3.1 Two-photon absorption (TPA) measurements

Polycrystalline ZnSe with a thickness of 3 mm was used to study the TPA process. In the experiment, the sample position was offset from the focus of lens L_9 to obtain a pump spot of ~ 2 mm, which completely covered the probe spot (~ 0.8 mm in the x -direction and $\sim 23 \mu\text{m}$ in the y -direction). The pump and probe energies are $10 \mu\text{J}$ and 3 nJ , respectively. The TPA process derives from the bound electron response to an external photoelectric field and typically occurs within a few femtoseconds. Therefore,

the dynamic trace of the TPA represents the cross-correlation between the pump pulse and probe pulse in our experiment. It can determine the minimum time resolution of our system and calibrate the time window. In the experiment, four sets of images were acquired: i) the grating image when both the pump and probe beams were turned on, i.e., the “pump on” image; ii) the grating image when the pump beam was turned off while the probe beam was turned on, i.e., the “pump off” image; iii) the environmental background when both the pump and probe beams were turned off; and iv) the pump beam background when the pump beam was turned on while the probe beam was turned off. As shown in Fig. 3, a set of grating images was obtained when the time delay stage at different z-positions (as indicated by the arrow in Fig. 1).

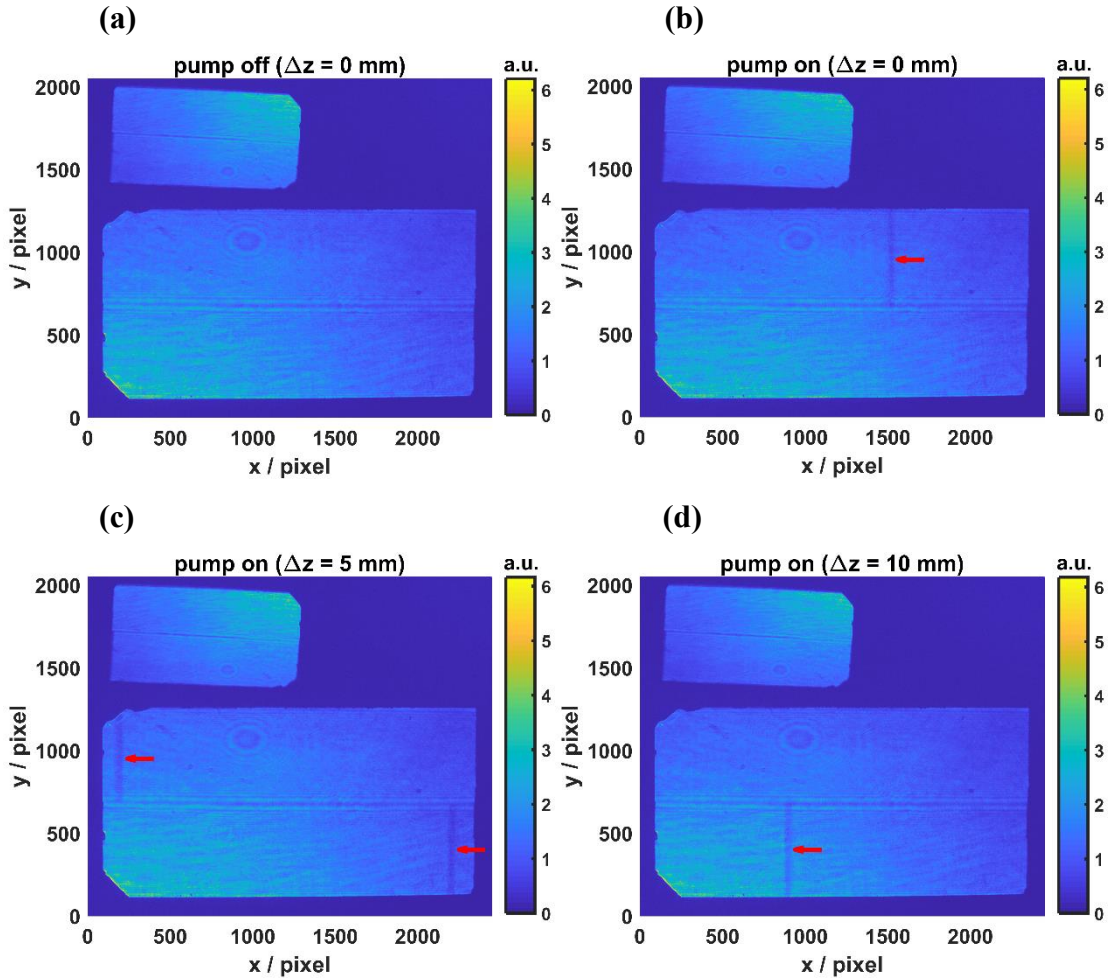


Fig. 3. (a) “Pump off” image at $\Delta z = 0$ mm; (b) “Pump on” image at $\Delta z = 0$ mm; (c) “Pump on” image at $\Delta z = 5$ mm; (d) “Pump on” image at $\Delta z = 10$ mm. The red arrow indicates the movement direction of the time delay.

In Fig. 3(a), a clear grating image of the “pump off” is shown and the environmental

background was subtracted. The upper part is the reference image, and the lower part is the signal image. As mentioned in Section 2, the reference image is inverted relative to the signal image and reduced by a factor of 2. The grating is divided into two rows by the reflection echelon with a narrow diffraction boundary. Therefore, the first (upper) and second (lower) rows have different time delays. In addition, the grating intensity distribution is not completely uniform. This does not affect the measurement results, as the probe beam is much weaker than the pump beam, and the intensity variation is normalized and corrected in the subsequent data processing. The corresponding "pump on" image is shown in Fig. 3(b). Similarly, we subtracted the pump beam background. A strip region appears (indicated by the red arrow), which is due to the TPA process when the probe beam and pump beam meet (zero-delay point). We set the z-position of the time delay stage as $\Delta z = 0$ mm and change it. The "pump on" images at $\Delta z = 5$ mm and 10 mm were obtained as shown in Fig. 3(c) and 3(d), corresponding to time delay increases of 33.3 ps and 66.7 ps, respectively. The movement of the TPA indicates that the time delay of the grating increases from the right to the left and from the first row to the second row, as indicated by the direction of the red arrow. In addition, the TPA appears in both the first and second rows at $\Delta z = 5$ mm. This is as we expected due to the overlap in the time windows of the two rows.

To extract the dynamic traces of ZnSe, the first and second rows were processed separately as follows:

$$T_{nor}^S = \frac{S_{11} - S_{10}}{S_{01} - S_{00}} \quad (3-1)$$

$$T_{nor}^R = \frac{R_{11} - R_{10}}{R_{01} - R_{00}} \quad (3-2)$$

$$T_{cor} = \frac{T_{nor}^S}{T_{nor}^R} \quad (3-3)$$

Here, S and R represent the signal image and reference image, respectively. For the first subscript, "1" means "pump on", and "0" means "pump off". Similarly, for the second subscript, "1" means "probe on", and "0" means "probe off". T_{nor}^S and T_{nor}^R represent the normalized transmittance of the signal image and reference image, respectively. It should be noted that the raw data amount of T_{nor}^R is only half of the amount of T_{nor}^S since the reference image is reduced by a factor of 2. Therefore, we integrate the pixels along the y-axis and then perform linear interpolation for T_{nor}^R . The corrected signal

trace T_{cor} is obtained by dividing T_{nor}^S by T_{nor}^R . In Fig. 4(a), we present the extracted traces of Fig. 3(a) and 3(b), where $\Delta z = 0$ mm. The left and right graphs are the traces of the first and second rows, respectively.

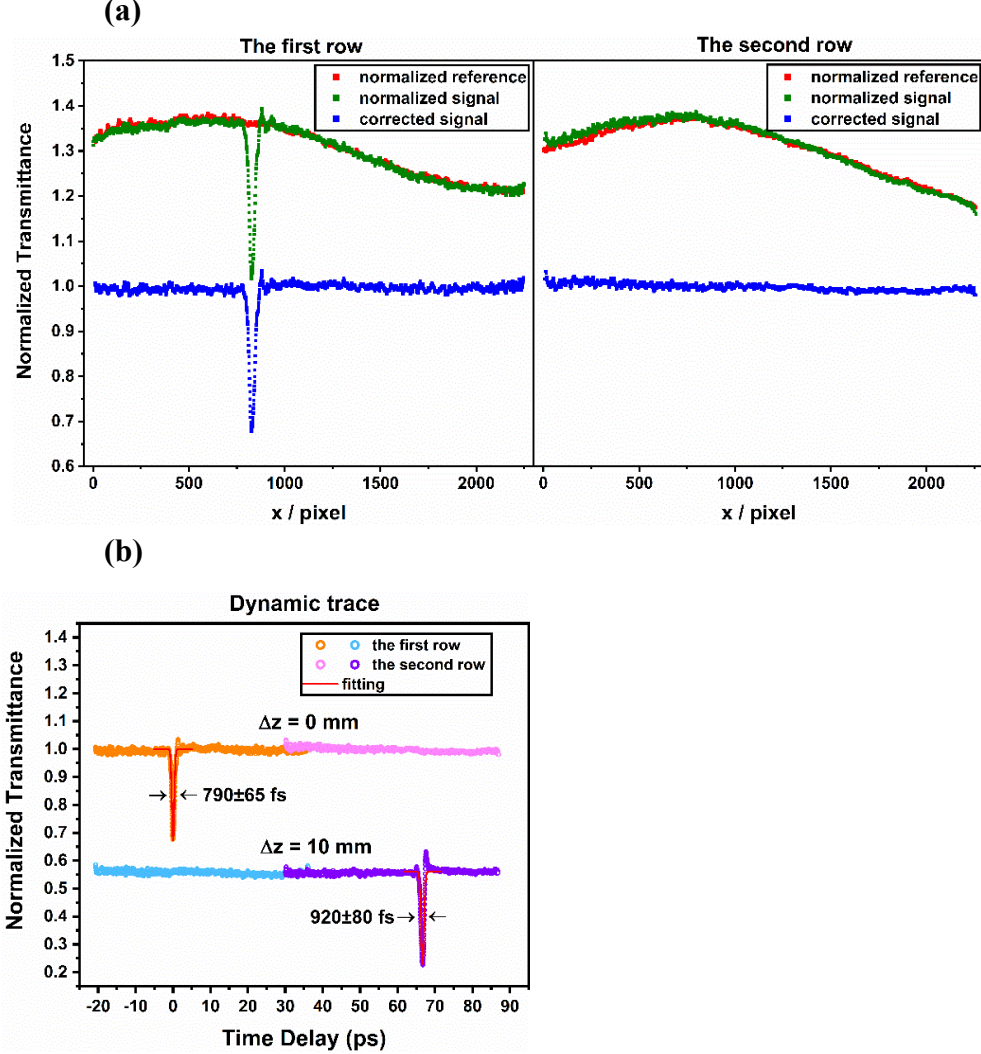


Fig. 4. (a) Extracted traces of ZnSe at $\Delta z = 0$ mm from the first and second rows. Green square: normalized signal trace; red square: normalized reference trace; blue square: corrected signal trace. (b) Complete single-shot dynamic traces of ZnSe at $\Delta z = 0$ mm and 10 mm, respectively. Orange and blue hollow circles: extracted traces at $\Delta z = 0$ mm and 10 mm from the first row, respectively; pink and purple hollow circles: extracted traces at $\Delta z = 0$ mm and 10 mm from the second row, respectively; red solid lines: theoretical fitting.

To make it easier to observe, we offset the y coordinates of the curve appropriately. Taking the first row as an example, the normalized signal trace T_{nor}^S (green square) has a significant TPA valley. However, there is a large fluctuation in the baseline even

after normalization. This is due to the spatial fluctuations between the "pump on" and "pump off" images since we acquired them by two independent pulses. Therefore, to correct spatial fluctuations, a reference image is necessary. As expected, the normalized reference trace T_{nor}^R (red square) conforms well to the normalized signal trace T_{nor}^S on the baseline. Therefore, dividing T_{nor}^S by T_{nor}^R eliminates the spatial fluctuations from pulse to pulse and yields the corrected signal trace T_{cor} (blue square). In addition, the first and second rows exhibit similar spatial fluctuations. This is because we integrate the pixels along the y -axis and retain only the spatial fluctuations along the grating length (x -axis). The same processing steps were implemented for Fig. 3c and Fig. 3d. By comparing the positions of the TPA valley, we determined that the time resolution per unit pixel in both the first and second rows is ~ 25.3 fs/pixel along the x -axis. Therefore, the time window of each row is ~ 57 ps and the total time window is ~ 109 ps. This is consistent with the calculated values in the Section 2. In Fig. 4(b), we present the complete single-shot dynamic traces of ZnSe at $\Delta z = 0$ mm and 10 mm after calibrating the time window. Both traces exhibit an ultrafast TPA process within the time window of 109 ps. And from $\Delta z = 0$ mm to 10 mm, the TPA valley shifted by ~ 66.7 ps. We can use a simple Gaussian function to fit the TPA trace of ZnSe:

$$T_{normalized} = 1 + A_0 \exp \left(- \left(\frac{t}{\tau_{TPA} / 2\sqrt{\ln 2}} \right)^2 \right) \quad (3-4)$$

where A_0 is a constant determined by the amplitude of the TPA and τ_{TPA} is the FWHM of the TPA valley. The fitting curves are shown in Fig. 4(b) with red solid lines. The fitting parameters A_0 and τ_{TPA} are -0.325 and 790 ± 65 fs and -0.330 and 920 ± 80 fs for the first and second rows, respectively. The average τ_{TPA} is ~ 855 fs, which is approximately 3 times the pulse cross-correlation width (269 fs, $\sqrt{2}$ times 190 fs (FWHM)). τ_{TPA} also represents the minimum time resolution in our experiment. Several factors can cause a broadening of the laser pulse or extend the time resolution, and these factors are discussed in Section 4.

3.2 Excited-stated absorption (ESA) measurements

Under the same experimental conditions, a symmetrical phenoxazinium bromine salt/DMF solution [20] with a concentration of 1.60 mg/mL was placed in a quartz cuvette with a thickness of 2 mm to study the ESA process. To better show the intensity change in the signal image, Fig. 5(a) shows the differential signal image ΔI_{signal} of the "pump on" and "pump off" images at a pump pulse energy of 19.58 μ J. A significant decrease

in the light intensity is observed from the first row to the second row. This indicates that the ESA process of the symmetrical phenoxazinium bromine salt should have a long life. Using the same steps as in Section 3.1, we separately extracted the dynamic traces from the first row and second row. The complete single-shot dynamic trace of the symmetrical phenoxazinium bromine salt is shown in Fig. 5(b). The dynamic trace of the first row (blue solid line) exhibits a fast recovery process, whereas that of the second row (green solid line) becomes slower. Therefore, the complete dynamic trace can be fitted using a double-exponential function:

$$T_{normalized} = 1 + A_1 \exp\left(-\frac{t}{\tau_1}\right) + A_2 \exp\left(-\frac{t}{\tau_2}\right) \quad (3-5)$$

where A_1 , τ_1 and A_2 , τ_2 are the amplitudes and lifetimes of the fast and slow processes, respectively. The fitting curve is also shown in Fig. 5(b) with the black solid line. The fitting parameters A_1 , τ_1 and A_2 , τ_2 are -0.05, 22 ± 10 ps and -0.05, > 1 ns, respectively. The two fitted life parameters can be attributed to the singlet excited state S_1 and the higher singlet excited state S_2 in the symmetrical phenoxazinium bromine salt. This result is consistent with the reports in [20] using a transient absorption spectrum and in [21] using a two-dimensional reflection echelon. Therefore it validates the effectiveness of our technique for the measurement of long-life dynamic processes. We can define the single-shot signal-to-noise ratio (SNR) of the measurement as $SNR = \Delta T / 2\sigma$; here, we take ΔT as the average normalized transmittance change of the slow process (time delay $t_d > 70$ ps), and σ is the standard deviation in this region. Therefore, SNR is ~ 6.4 in our experiment. Moreover, if we set $SNR = 1$, the minimum relative transmittance change that can be detected in a single-shot is $\sim 0.75\%$ in our experiment.

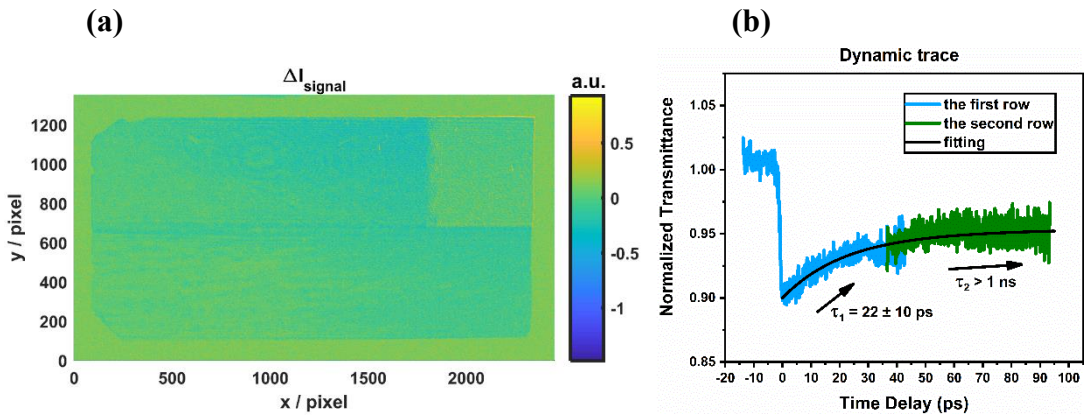


Fig. 5. (a) Differential signal image of the “pump on” and “pump off” images at a pump pulse energy

of 19.58 μJ . (b) Complete single-shot dynamic trace of the symmetrical phenoxazinium bromine salt/DMF solution. The solid blue line represents the extracted trace from the first row; the solid green line represents the extracted trace from the second row; and the solid black line represents the theoretical fitting.

4. Discussion

In Section 3.1, we obtained the average τ_{TPA} , i.e., the minimum time resolution is approximately 3 times the pulse cross-correlation width 269fs. One of the main factors that can significantly degenerate the time resolution is the angular spectral dispersion of the grating [19]. The angular spectral dispersion q causes a linear chirp of the pulse. Using Eq. (2-2), for $\beta=0$, the angular spectral dispersion is $q = d\beta/d\omega = -\sin\alpha/\omega$. Here, $\omega = 2\pi c/\lambda$ is the center angular frequency of the laser, and λ is the center wavelength. It is assumed that the lens and mirrors do not change the pulse width and the pulse broadening occurs only between the grating and the converging lens L_5 , as shown in Fig. 6(a).

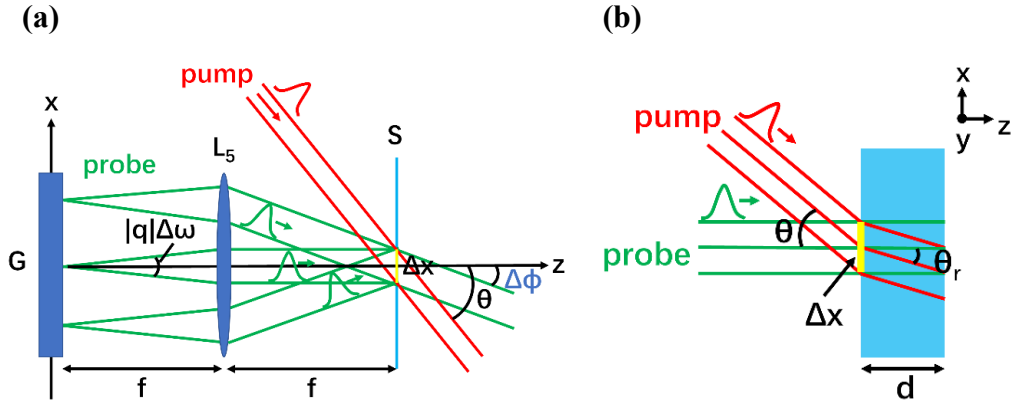


Fig.6. (a) Schematic of the angular spectral dispersion of the grating and beams crossing at the sample plane. (b) Enlarged schematic of the beam cross in the sample. G: grating; S: sample plane (focal plane); Δx : probe spot on the sample; $\Delta\Phi$: angular rotation of the probe beam; θ : cross angle of the pump and probe; θ_r : refraction angle of the pump beam within the sample; d : sample thickness.

The pulse width τ (half width at $1/e$ height) in the sample plane S (back-focal plane of lens L_5) can be expressed as [19]:

$$\tau = \tau_0 \left[1 + (t_c / \tau_0)^4 \right]^{1/2} \quad (4-1)$$

This formula assumes that the initial pulse has a Fourier transform-limited form

$I(t) = I_0 \exp(-t^2 / \tau_0^2)$, where τ_0 is the initial pulse width (half width at 1/e height). t_c is the characteristic time of the experimental setup:

$$t_c = \left(\frac{|q|T}{2 \sin^{-1} NA} \right)^{1/2} \quad (4-2)$$

Here, T is the time window for the grating, $NA = \sin(L_{eff} / 2f)$ is the numerical aperture of lens L_5 , L_{eff} is the effective length of the grating, and f is the focal length of lens L_5 . In our experiments, $\alpha \sim 44^\circ$, $T \sim 56$ ps, $\lambda = 515$ nm, $L_{eff} = 24$ mm, $f = 250$ mm, and τ_0 is assumed to be 114 fs ($190\text{fs}(\text{FWHM}) / 2\sqrt{\ln 2}$). Therefore, using Eqs. (4-1) and (4-2), we can derive that t_c and τ are 332 fs and 974 fs, respectively.

The second factor that needs to be considered is the cross angle between the pump and probe beams on the sample surface. As shown in Fig. 6(a), we assume that the pump and probe beams are in the xz plane with an angle θ . For convenience, we ignore the small angular rotations $\Delta\Phi$ of the probe beam [19], $\sim \pm 2.7^\circ$ in our setup. The probe spot Δx in the sample plane depends on the spectral width $\Delta\omega$ of the probe beam. For a Gaussian pulse, $\Delta x = |q| \Delta\omega f = 2f \sin \alpha / \omega \tau_0$. It should be noted that adding a reflection echelon orthogonal to the grating changes only the probe spot Δy in the y -direction, so it does not affect the time resolution. Therefore, the extension of the time resolution by beam cross can be expressed as follows:

$$\Delta t_c = \Delta x \sin \theta / c \quad (4-3)$$

In our experiments, the probe spot Δx is ~ 0.83 mm and θ is $\sim 33.6^\circ$. Δt_c can be calculated as 1531 fs. In addition, the thickness of the sample can also lead to an extension of the time resolution [7]. Assuming that the sample thickness is d and the refraction angle of the pump beam is θ_r , as shown in Fig. 6(b), the extension of the time resolution Δt_s due to the sample thickness can be expressed as follows:

$$\Delta t_s = d [(\sin \theta_r \sin \theta - 1) / \cos \theta_r + 1] / c \quad (4-4)$$

Here, θ_r and θ are correlated by the law of refraction. In our experiments, the refractive index of ZnSe is ~ 2.7 , the thickness d is 3 mm, and θ_r is $\sim 11.8^\circ$; therefore, Δt_s can be calculated as 940 fs. Overall, the equivalent pulse width is $\tau_{probe} = (\tau^2 + \Delta t_c^2 + \Delta t_s^2)^{1/2} = 2044$ fs. The minimum time resolution τ_R of a chirped pulse is given by [22]:

$$\tau_R = \sqrt{\tau_0 \sqrt{\tau^2 - \tau_0^2}} \quad (4-5)$$

In a long chirp limit, this resolution is equivalent to the minimum time resolution $\tau_R = \sqrt{\tau_0 \tau}$ in a spectrally encoded strategy. Using Eq. (4-5), we can derive $\tau_R = 482$ fs (811 fs, FWHM). We assumed that the pump pulse width τ_{pump} is maintained at 190 fs (FWHM), that the convolution of the pump pulse and the broadened probe pulse results in a time resolution of $\tau_{con} = (\tau_R^2 + \tau_{pump}^2)^{1/2} = 825$ fs (FWHM), and that this value is close to the average $\tau_{TPA} \sim 855$ fs that we measured. Other factors that may broaden the pulse width include the group velocity dispersion (GVD) of the sample, which also depends on the sample thickness. Overall, as seen from the above analysis, to obtain a short time resolution while maintaining a large time window, we need to increase the numerical aperture NA of the converging lens L_5 (reduce the characteristic time t_c), reduce the angle θ between the pump and probe beams, and use a thinner sample.

In addition, although we chose a degenerate wavelength 515 nm pump-probe scheme, different pump-probe wavelengths and polarizations can be selected according to the experimental requirements. Similar to the echelon encoding [3, 14] or the angle beam encoding strategy [1, 2, 8], the grating encoding strategy can also implement single-shot transient absorption spectroscopy. This requires the use of a white light probe and the addition of a spectrometer in front of the CCD. The spectrum is decomposed in the y -direction, which is perpendicular to the grating time-axis (x -direction). In this way, therefore, the time dimension in the y -direction should be replaced by the spectral dimension, which limits the available time window to approximately 50-60 ps.

In this study, we focused mainly on the report of a single-shot pump-probe technique with a large time window and accurate imaging. In the current configuration, we only accurately image the grating plane on the CCD, not the reflection echelon. Therefore, there is a diffraction pattern similar to the interference fringes between the rows of the grating (as shown in Fig. 3). In the data processing, we simply discarded the data in this region because the data occupy only a small part of the grating and do not affect the processing results. In our experiment, the distance between the grating and the echelon is ~ 270 mm. This distance is only limited by the interference between the optical elements in the experiment and can be shortened as much as possible. Another method is to add a 4f imaging system between the reflection echelon and the grating to project the echelon image onto the grating surface. Therefore, even though a two-step echelon was used in this study, more steps can be used, such as four steps, which would increase the total time window to more than 200 ps.

5. Conclusion

We demonstrated a single-shot pump-probe technique by combining a reflection echelon and a commercial grating. A large time window of ~ 109 ps is obtained, and accurate imaging is maintained. The obtained time window exceeds the maximum reported values by using an angle beam or echelon encoding strategy. Studies of the TPA process of ZnSe and the ESA process of a symmetrical phenoxazinium bromine salt demonstrate either ultrafast or slow absorption dynamic processes, this technique can provide reliable measurements. The measured average minimum time resolution is ~ 855 fs, and the minimum relative transmittance change that can be detected in a single-shot is $\sim 0.75\%$. The time resolution is mainly limited by the angular spectral dispersion, beam cross, and sample thickness. This technique can also be modified to a wavelength-resolved technique or to further increase the time window to more than 200 ps. In summary, using the echelon and grating combination strategy, a single-shot pump-probe technique with a large time window is achieved for diagnosing various dynamic processes ranging from subpicoseconds to hundreds of picoseconds.

Acknowledgements.

We gratefully acknowledge the National Natural Science Foundation of China (11704273, 51607119), National Safety Academic Fund (U1630103), and Science and Technology Innovation Team of Guizhou Education Department (Grant No. [2023]094).

Declaration of interest.

The authors declare no conflicts of interest.

References

1. Y. Minami, H. Yamaki, I. Katayama, *et al.*, “Broadband pump–probe imaging spectroscopy applicable to ultrafast single-shot events,” *Appl. Phys. Express.* **7**(2), 022402(2014). <https://doi.org/10.7567/APEX.7.022402>.
2. N. Furukawa, C. E. Mair, V. D. Kleiman, *et al.*, “Femtosecond real-time pump–probe imaging spectroscopy,” *Appl. Phys. Lett.* **85**(20), 4645-4647(2004). <https://doi.org/10.1063/1.1823039>.
3. J. Takeda, W. Oba, Y. Minami, *et al.*, “Ultrafast crystalline-to-amorphous phase transition in Ge₂Sb₂Te₅ chalcogenide alloy thin film using single-shot imaging spectroscopy,” *Appl. Phys. Lett.* **104**(26), 261903(2014). <https://doi.org/10.1063/1.4886969>.

4. K. Mishchik, C. J. Leger, O. D. Caulier, *et al.*, “Ultrashort pulse laser cutting of glass by controlled fracture propagation,” *J. Laser Micro Nanoeng.* **11**(1), 12(2016).
<https://doi.org/10.2961/jlmn.2016.01.0012>.
5. G. P. Wakeham and K. A. Nelson, “Dual-echelon single-shot femtosecond spectroscopy,” *Opt. Lett.* **25**(7), 505-507(2000). <https://doi.org/10.1364/OL.25.000505>.
6. L. Dhar, J. T. Fourkas and K. A. Nelson., “Pulse-length-limited ultrafast pump–probe spectroscopy in a single laser shot,” *Opt. Lett.* **19**(9), 643-645(1994).
<https://doi.org/10.1364/OL.19.000643>.
7. K. S. Wilson and C. Y. Wong., “Single-shot transient absorption spectroscopy with a 45 ps pump-probe time delay range,” *Opt. Lett.* **43**(3), 371-374(2018).
<https://doi.org/10.1364/OL.43.000371>.
8. K. S. Wilson, A. N. Mapile, and C. Y. Wong, “Broadband single-shot transient absorption spectroscopy,” *Opt. Express.* **28**(8), 11339-11355(2020). <https://doi.org/10.1364/OE.390938>.
9. M. Kobayashi, Y. Arashida, G. Yamashita, *et al.*, “Fast-frame single-shot pump-probe spectroscopy with chirped-fiber Bragg gratings,” *Opt. Lett.* **44**(1), 163-166(2019).
<https://doi.org/10.1364/OL.44.000163>.
10. M. Kobayashi, Y. Arashida, K. Asakawa, *et al.*, “Pulse-to-pulse ultrafast dynamics of highly photoexcited Ge₂Sb₂Te₅ thin films,” *Jpn. J. Appl. Phys.* **62**(2), 022001(2023).
<https://doi.org/10.35848/1347-4065/acb476>.
11. G. S. Beddard, G. G. McFadyen, G. D. Reid, *et al.*, “Pulse transform transient absorption spectroscopy,” *Chem. Phys. Lett.* **198**(6), 641-644(1992). [https://doi.org/10.1016/0009-2614\(92\)85042-9](https://doi.org/10.1016/0009-2614(92)85042-9).
12. I. A. Shkrob, D. A. Oulianov, R. A. Crowell, *et al.*, “Frequency-domain “single-shot” ultrafast transient absorption spectroscopy using chirped laser pulses,” *J. Appl. Phys.* **96**(1), 25-33(2004). <https://doi.org/10.1063/1.1711178>.
13. T. Shin, J. W. Wolfson, S. W. Teitelbaum, *et al.*, “Dual echelon femtosecond single-shot spectroscopy,” *Rev. Sci. Instrum.* **85**(8), 083115(2014). <https://doi.org/10.1063/1.4893641>.
14. I. Katayama, H. Sakaibara, and J. Takeda, “Real-Time Time–Frequency Imaging of Ultrashort Laser Pulses Using an Echelon Mirror,” *Jpn. J. Appl. Phys.* **50**(10R), 102701(2011). <https://doi.org/10.1143/JJAP.50.102701>.
15. Z. Jin, A. Wada, J. H. Shin, *et al.*, “A Single-shot Terahertz Time-domain Spectroscopy Instrument for Intense Laser System,” in *Journal of Physics: Conference Series*, **688**(1), 012040(2016). <https://doi.org/10.1088/1742-6596/688/1/012040>.
16. L. Yan, X. Wang, J. Si, *et al.*, “Multi-frame observation of a single femtosecond laser pulse

- propagation using an echelon and optical polarigraphy technique,” IEEE Photon. **25**(19), 1879-1881(2013). <https://doi.org/10.1109/LPT.2013.2278883>.
17. L. Zanotto, G. Balistreri, A. Rovere, *et al.*, “Terahertz scanless hypertemporal imaging,” Laser Photonics Rev. **17**(8): 2200936(2023). <https://doi.org/10.1002/lpor.202200936>.
 18. J. Zhao, J. Dai, B. Braverman, *et al.*, “Compressive ultrafast pulse measurement via time-domain single-pixel imaging,” Optica. **8**(9), 1176-1185(2021). <https://doi.org/10.1364/OPTICA.431455>.
 19. A. Spiro and M. Lowe, “Method of ultrafast beam rotation for single-shot, time-resolved measurements,” Opt. Lett. **39**(18), 5362-5365(2014). <https://doi.org/10.1364/OL.39.005362>.
 20. Z. Xiao, J. Ge, Z. Li, *et al.*, “Ultrafast optical limiting properties and transient dynamics of symmetrical phenoxazinium bromine salt,” Opt. Mater. **50**, 263-267(2015). <https://doi.org/10.1016/j.optmat.2015.10.033>.
 21. J. Yang, W. Zhou, F. Wang, *et al.*, “Single-shot pump-probe technique using mirror array,” APPL PHYS B-LASERS O. **126**, 1-5(2020). <https://doi.org/10.1007/s00340-020-07446-z>.
 22. K. J. Garriga Francis and X. C. Zhang, “Local measurement of terahertz field-induced second harmonic generation in plasma filaments,” Front. Optoelectron. **16**(1), 44(2023). <https://doi.org/10.1007/s12200-023-00095-y>.